

Buckling instabilities of subducted lithosphere beneath the transition zone

N.M. Ribe^{a,*}, E. Stutzmann^a, Y. Ren^a, R. van der Hilst^b

^a Institut de Physique du Globe, UMR 7154 CNRS, 4, Place Jussieu, 75252 Paris cédex 05, France

^b Department of Earth, Atmospheric and Planetary Sciences, MIT, 77 Massachusetts Ave., Cambridge, MA 02139, USA

Received 27 June 2006; received in revised form 31 October 2006; accepted 18 November 2006

Available online 26 December 2006

Editor: G.D. Price

Abstract

A sheet of viscous fluid poured onto a surface buckles periodically to generate a pile of regular folds. Recent tomographic images beneath subduction zones, together with quantitative fluid mechanical scaling laws, suggest that a similar instability can occur when slabs of subducted oceanic lithosphere encounter enhanced resistance to penetration at 660 km depth. Beneath subduction zones such as Central America and Java, the fast anomalies in elastic wavespeed are too broad (≥ 400 km) to be explained by simple compressional thickening of subducted lithosphere that is initially 50–100 km thick. By contrast, a periodic buckling mechanism can account for both the characteristic ‘wedge’ shapes of the anomalies and for their widths, which agree closely with those predicted by the scaling laws. In addition to providing a plausible physical interpretation of tomographic observations beneath some subduction zones, buckling instabilities have important consequences for other aspects of global geodynamics such as tectonic plate reconstructions, interpretation of geoid anomalies, and modeling of secular changes in Earth’s moment of inertia.

© 2006 Elsevier B.V. All rights reserved.

Keywords: Subduction; Seismic tomography; Buckling instabilities

1. Introduction

All home cooks are familiar with the beautiful ‘periodic buckling’ instability of a sheet of cake batter, molten chocolate, or honey that is poured onto a surface (Fig. 1a). Recent tomographic images of the earth’s interior, together with quantitative scaling laws derived from fluid mechanics, suggest that a similar instability can occur when a slab of oceanic lithosphere encounters enhanced resistance to penetration at 660 km depth.

The buckling of a viscous sheet is a classic problem in fluid mechanics, and the history of its investigation spans nearly 40 yr. The most commonly studied configuration (Fig. 1a) involves a sheet with viscosity μ , density anomaly $\Delta\rho$, and initial thickness d_0 that is injected downward at speed U_0 and falls a distance H through air onto a rigid surface. Taylor [1] first pointed out that fluid buckling, like its elastic analog, requires a longitudinal compressive stress. Extensive laboratory experiments on periodic buckling on a solid surface were performed by Cruickshank [2], and on fluid/fluid interfaces by Griffiths and Turner [3]. Subsequently, the critical fall height for the onset of buckling was

* Corresponding author. Tel.: +33 1 44272479; fax: +33 1 44272481.
E-mail address: ribe@ipgp.jussieu.fr (N.M. Ribe).

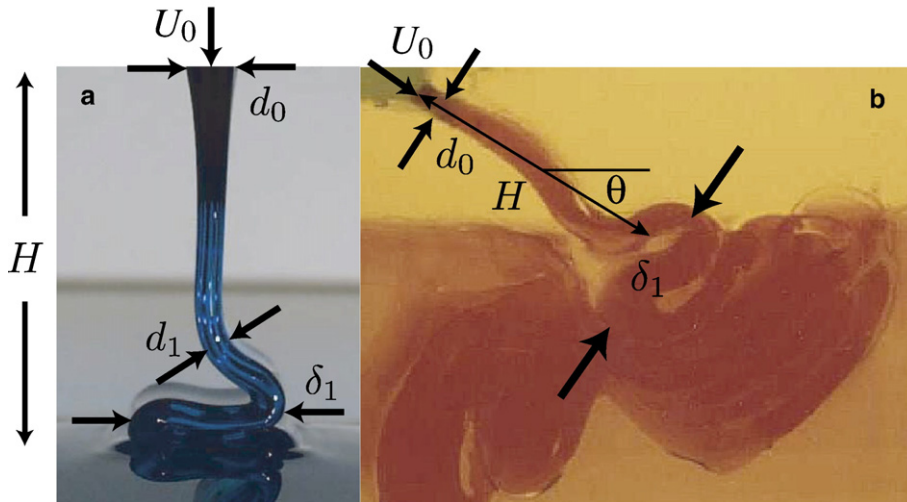


Fig. 1. Periodic buckling of sheets of viscous corn syrup. (a) The most common experimental configuration, in which a sheet with viscosity μ , density anomaly $\Delta\rho$, and initial thickness d_0 is injected downward at speed U_0 and falls a distance H through air onto a rigid surface (photograph by N. Ribe). The thickness of the buckling portion of the sheet is d_1 , and the total amplitude of the folds is δ_1 . (b) A more geophysically realistic configuration [10] in which the sheet is injected obliquely into a tank containing two superposed layers of viscous corn syrup, and buckling occurs at the interface between the layers. Here $\mu=7\times 10^5$ Pa s, $\Delta\rho=58$ kg m $^{-3}$, $d_0=0.01$ m, $\theta=35^\circ$, $U_0=5\times 10^{-4}$ m s $^{-1}$, and $H=0.0925$ m. The red mass of fluid at lower left was formed by an episode of buckling earlier in the experiment. (photograph courtesy of L. Guillou-Frottier).

determined by linear stability analysis [4,5]. The first numerical simulations of finite-amplitude periodic buckling were performed by Tome and McKee [6] using a marker-and-cell method. Skorobogatiy and Mahadevan [7] proposed scaling laws for the amplitude and frequency of finite-amplitude buckling driven by gravity, and validated the results using laboratory experiments and a numerical model for an inextensible sheet. Ribe [8], using a more realistic numerical model that allowed for extensional deformation, documented the existence of a second buckling mode and determined complete scaling laws for the buckling amplitude and frequency in the absence of inertia.

Griffiths and Turner [3] were the first to suggest that periodic buckling might occur when subducted lithosphere interacts with a viscosity and/or density interface at 660 km depth in the mantle. Since then, several numerical and experimental studies have shown that buckling instabilities can occur in more realistic subduction-like situations. Gaherty and Hager [9] observed periodic buckling in a numerical model of subducted compositional lithosphere impinging on an interface with a viscosity jump. Guillou-Frottier, Buttles and Olson [10] performed laboratory experiments on the subduction of dense slabs of corn syrup into a two-layer ‘mantle’ with variable rates of imposed trench migration (‘rollback’). They observed buckling instabilities of the slab when its sinking speed in the upper layer and its horizontal speed in excess of the rollback speed both

greatly exceeded the sinking speed in the lower layer. Christensen [11] found similar instabilities in a numerical study of the same system. Buckling of subducted lithosphere has also been observed in numerical studies with more complex geometries and rheologies [12,13,14] and in laboratory experiments on free subduction [15]. However, none of these studies determined quantitative scaling laws for the amplitude or frequency of the buckling.

Here we use the scaling laws of Ribe [8] to test quantitatively the hypothesis that subducted lithosphere may undergo buckling instabilities beneath the transition zone. The relevance of the scaling laws to subduction-like geometries is first demonstrated by comparing their predictions with experimental observations of buckling in a two-layer fluid system [10]. We then show that the scaling laws predict buckling amplitudes that agree well with those that can be inferred from tomographic images of subduction beneath Central America and Java. To conclude, we discuss the broader implications of the results for other aspects of global geodynamics, including tectonic plate reconstructions, interpretation of geoid anomalies, and modeling of secular changes in Earth’s moment of inertia.

2. Scaling laws for buckling

Fig. 2 summarizes the scaling laws for periodic buckling determined by Ribe [8] using a numerical

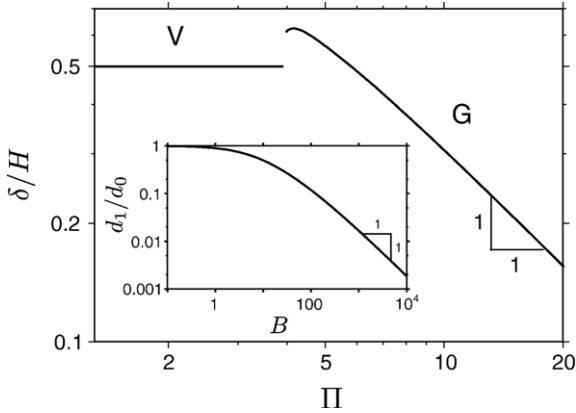


Fig. 2. Amplitude of periodic buckling of a viscous sheet in the absence of inertia [8]. Main part: midsurface amplitude δ normalized by the fall height H , as a function of the dimensionless parameter Π defined by Eq. (1). Branches corresponding to viscous and gravitational buckling are denoted by V and G, respectively. Inset: gravitational thinning factor d_1/d_0 as a function of the buoyancy number $B = g\Delta\rho H^2/\mu U_0$.

model based on thin-sheet theory. When fluid inertia is negligible, two distinct modes of buckling can occur, depending on the value of a dimensionless parameter

$$\Pi = H(g\Delta\rho/\mu U_1 d_1^2)^{1/4} \quad (1)$$

that measures the importance of gravity. Here d_1 is the thickness of the sheet in the region where the buckling occurs (Fig. 1a), and $U_1 = U_0 d_0/d_1$ is the corresponding axial velocity implied by steady-state conservation of mass. When Π is below a critical value $\Pi_c \approx 3.9$, gravity can be neglected, and buckling occurs in a ‘viscous’ mode in which the net viscous force on each element of the sheet is zero. The amplitude of viscous buckling (measured from the sheet’s midsurface) is $\delta \approx 0.50H$ (segment ‘V’, main part of Fig. 2). At $\Pi = \Pi_c$, the buckling bifurcates to a ‘gravitational’ mode in which the viscous forces that resist the bending of the sheet are balanced by gravity (segment ‘G’, main part of Fig. 2). In the limit $\Pi \gg \Pi_c$, the amplitude of gravitational buckling is $\delta \approx 3.2(\mu d_1^2 U_1/g\Delta\rho)^{1/4} \equiv 3.2H\Pi^{-1}$ [7,8].

The unknown thickness d_1 that appears in Eq. (1) can be determined analytically using a simple model for a vertical sheet falling under gravity [8]. The ratio d_1/d_0 depends only on the ‘buoyancy number’ $B \equiv g\Delta\rho H^2/\mu U_0$, and is shown as a function of B in the inset of Fig. 2. By combining the two parts of Fig. 2, one can predict the midsurface amplitude δ and the total amplitude $\delta_1 = \delta + d_1$ for any given values of μ , $\Delta\rho$, d_0 , U_0 and H .

Although the scaling laws of Fig. 2 were derived for a sheet falling vertically, they remain valid in more realistic subduction-like geometries. To demonstrate

this, we compare the buckling amplitude predicted by the scaling laws with the amplitude observed in the analog laboratory experiment shown in Fig. 1b. Substituting the known values of μ , $\Delta\rho$, d_0 , U_0 and H (caption of Fig. 1) into the scaling laws of Fig. 2, we find $\delta_1 = 0.057$ m, within 2% of the observed value $\delta_1 = 0.056$ m. Because $\Pi = 0.95$ for this experiment, the buckling occurs in the ‘viscous’ regime.

A further important point illustrated by Fig. 1b is that buckling instabilities typically produce not just a single fold, but rather a ‘pile’ of superposed folds that widens downward due to gravitational collapse. This pile has a characteristic pyramidal or ‘wedge’ shape whose width at the top is δ_1 , the amplitude of the most recently formed fold.

An assumption inherent in the scaling laws of Fig. 2 is that the fluid surrounding the sheet has a negligible influence on the buckling. The validity of this assumption can be tested using a simple scaling analysis. The viscous stress within a buckling lithosphere of thickness d is $\sigma \sim \mu d^3 U/\delta^4$, where U is the characteristic velocity of the deformation. The stress in the ambient fluid (with viscosity μ_0) is $\sigma_0 \sim \mu_0 U/\delta$. The viscosity of the outer fluid can be neglected if $\sigma_0 \ll \sigma$, or $\mu/\mu_0 \gg (\delta/d)^3$. For typical buckling amplitudes $\delta/d \approx 4-5$, the viscosity of the surrounding fluid will be negligible if $\mu/\mu_0 \gg 100$, which is probably the case for slabs in the upper and mid-mantle.

3. Seismic tomography

We turn now to the evidence provided by seismic tomography for strong apparent thickening of subducted lithosphere in the mid-mantle. Two examples are the subduction of the Cocos plate beneath Central America, and of the Australian plate beneath Java. Fig. 3 shows cross-sections beneath these subduction zones through two different tomographic models. The first is the global P-wave velocity model ‘KH’ [16], derived from reprocessed [17] P-wave travel time residuals published by the International Seismological Centre (ISC), together with about 1900 PKP and Pdiff differential travel times measured by waveform cross-correlation. The model is parametrized using irregular cells with minimum lateral dimensions $0.7^\circ \times 0.7^\circ$ and radial extent 150 km. The iterative LSQR algorithm was used to invert the differential travel times to retrieve the P-wave slowness perturbations. The second (‘RSHB’) model is a regional P- and S-wave velocity model restricted to the region beneath the Americas [18]. This model is derived from 37,000 differential travel times of direct P and S waves and 2000 PcP-P and ScS-S times

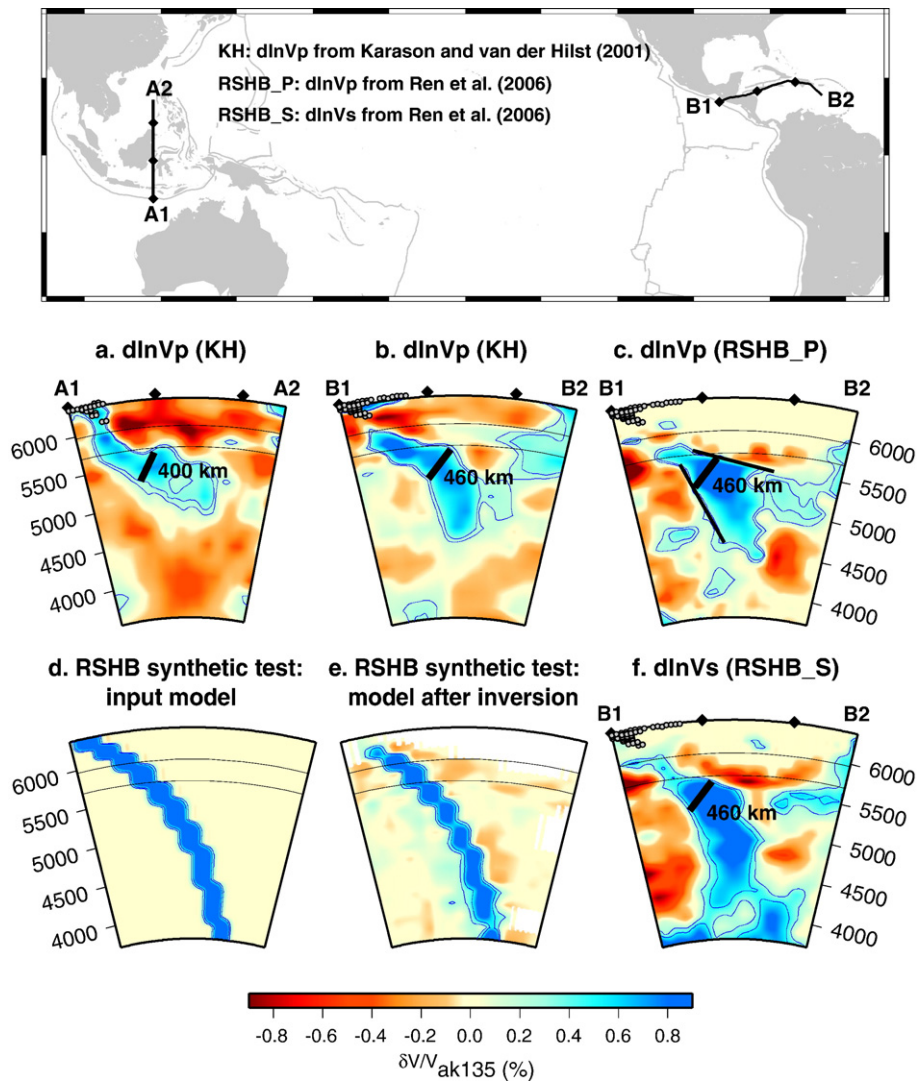


Fig. 3. Tomographic images of the subducted Australian plate beneath Java (profile A1–A2) and the Cocos plate beneath Central America (profile B1–B2). Images are derived from a global P-wave velocity model ‘KH’ [16] for both cross-sections, and from a regional P- and S- wave velocity model ‘RSHB’ beneath the Americas [18]. Colors show the deviations of the P- or S-wave speed relative to the laterally averaged reference model ak135 [19]. Because the amplitude of the P-wave velocity model is smaller than that of the S-wave model, the boundaries of the fast anomaly are indicated by contours of 0.2% and 0.3% (for P) and 0.4% and 0.5% (for S). The heavy black bars indicate the buckling amplitudes predicted using the scaling laws of Fig. 2. Panels d) and e) show a synthetic resolution test of the RSHB model. The input P-wave velocity model represents a slab 200 km wide and 1000 km long in the direction perpendicular to the image, and inversion is performed using the same path coverage as for the model RSHB. An analogous test using the S-wave data gives similar results (not shown).

measured by waveform cross-correlation on carefully selected broadband data. P-wave and S-wave data were inverted simultaneously to retrieve the slowness perturbations in a model parametrized in cells of $2^\circ \times 2^\circ \times 150$ km using the LSQR algorithm. The model resolution is uniform below 600 km depth but degraded above it, because only rays with turning points beneath the upper mantle discontinuities were retained in order to avoid the ambiguity of determining phase arrivals in the

triplification range. The profiles A1–A2 and B1–B2 along which the cross-sections are taken are perpendicular at each point to the estimated past positions of the active margins for Java [20] and Central America [18]. This ensures that the subducted lithosphere is perpendicular to the cross-sections at each depth, thereby minimizing the spurious apparent thickening that results when the lithosphere is oblique to the section.

In all the cross-sections shown in Fig. 3, the subducted lithosphere below 660 km appears as a fast anomaly in the shape of an expanding ‘wedge’ whose width reaches 500–700 km in the mid-mantle. The borders of one of these wedges are indicated by black lines in Fig. 3c. To demonstrate that the apparent thickening is real, we performed a synthetic test using the same path coverage and regularization parameters as those used to construct the velocity model RSHB. The input velocity model for the test (Fig. 3d) represents a slab 200 km wide that extends down to the core–mantle boundary (CMB). After inversion, the narrow slab is still clearly visible, with very little spurious widening (Fig. 3e). This result shows that our path coverage would enable us to resolve a slab 200 km wide beneath Central America. Because the apparent thickness of the slab on the tomographic images is considerably greater than this (Fig. 3c, e), we conclude that it is real and not an artefact of the inversion. This conclusion is further strengthened by the similar shapes of the V_p and V_s anomalies for model RSHB in the mid-mantle beneath Central America (Fig. 3c, f). The differences between the two anomalies deeper in the lower mantle may reflect the fact that the anomalous wavespeed of slabs reaching these depths is primarily compositional rather than thermal in origin, and that S waves may be more sensitive to the former than P waves are [21].

We suggest that the wedge-like structures seen in the tomographic images are sinking ‘piles’ of folds generating by buckling instabilities in the transition zone. To test this hypothesis quantitatively, we use the scaling laws of Fig. 2 to predict the total buckling amplitude δ_1 beneath Central America and Java. The initial thicknesses $d_0=45$ km (Central America) and 80 km (Java) correspond to the depths to the 1100 °C isotherm for the ages (≈ 20 –25 and ≈ 80 Ma, respectively) of the lithosphere now being subducted [22]. The corresponding plate convergence rates [23] are $U_0 \approx 6.3$ cm yr⁻¹ (Central America) and 7.9 cm yr⁻¹ (Java). The assumed density anomaly $\Delta\rho = \rho_0\alpha\Delta T = 65$ kg m⁻³ is that associated with a mean temperature anomaly $\Delta T = 550^\circ$ in a material with reference density $\rho_0 = 3400$ kg m⁻³ and thermal expansion coefficient $\alpha = 3.5 \times 10^{-5}$ K⁻¹. We choose $\mu = 10^{23}$ Pa s for the (poorly known) effective viscosity of the lithosphere, but the results depend only weakly on this parameter. The subduction angle $\theta \approx 65^\circ$ in both cases. The effective fall height is $H = H_1 / \sin \theta$, where $H_1 = 660$ km – d_0 is the thickness of the upper mantle below the lithosphere, and the effective gravitational acceleration in the downdip direction is $g \sin \theta$. With these values, the scaling laws of Fig. 2 predict $\delta_1 = 460$ km for Central America and

$\delta_1 = 400$ km for Java. These widths are indicated by the black bars in Fig. 3a–c and Fig. 3f, and correspond very well to the widths of the observed seismic velocity anomalies just below the transition zone.

4. Discussion

The apparent thickening of the slab in the tomographic images – equivalent to about five times the slab thickness – is too large to be easily explained by a mechanism other than buckling. The principal alternative, sometimes called ‘advective’ or ‘pure shear’ thickening, is uniform widening of the slab in response to the downdip compressional stress due to an increasing viscous resistance with depth. However, numerical models [24,9] show that this mechanism can thicken the slab by at most a factor of two, which is not sufficient to account for the tomographic observations. The amplitude of a buckling instability, by contrast, can easily attain values of several times the slab thickness. Moreover, the physical requirement for buckling to occur is easily met: in the geometry of Fig. 1a, for example, the instability sets in when the fall height exceeds only about 4 times the sheet thickness [4,5]. In the mantle, therefore, the critical fall height for lithosphere ≤ 80 km thick is only ≈ 320 km, which is exceeded whenever subducted lithosphere enters the transition zone (420–660 km depth). This might suggest that all subducted slabs should fold in the transition zone; yet tomographic images of subduction zones such as Izu Bonin do not show the apparent thickening of the lithosphere that is characteristic of buckling. The most likely reason is retrograde motion (‘rollback’) of the trench where the lithosphere plunges into the mantle. Laboratory experiments [10,25] show that buckling only occurs if the rollback speed is sufficiently small, because rollback tends to make a descending slab lie down flat on an interface, like toothpaste falling onto a toothbrush from a moving tube. This is consistent with the fact that both Central America and Java, where wedge-shaped velocity anomalies beneath the transition zone indicate that buckling may have occurred, have very low (<10% of the convergence speed) rates of trench rollback [23].

Although we have focused on Central America and Java, there are other subduction zones where buckling instabilities may also have occurred. Residual travel time anomalies from deep earthquakes are consistent with substantially thickened (by factors of up to five) slabs in the lower mantle beneath the Marianas, Kuril–Kamchatka, and Tonga subduction zones, although they do not uniquely require such thickening [26,27].

Analysis of seismic bodywaveforms suggests the presence of a 900-km thick slab in the mid-mantle beneath the east coast of North America [28]. Tomographic images also show significant slab thickening in the mid-mantle beneath central South America [29,18]. For an overview of slab-related velocity anomalies around the Pacific ocean, the reader is referred to the comprehensive review of Fukao et al. [30].

Even if a slab does not fold during its passage through the transition zone, it may do so at the core–mantle boundary (CMB), which due to its high density contrast is impermeable to sinking mantle material. Buckling at the CMB would produce piles of folded lithosphere there, similar in appearance to those in Fig. 1. We speculate that some of the fast seismic velocity anomalies in the lowermost mantle may be due to such ‘fold piles’; possible examples include the anomalies beneath Japan/Eastern China [16] and the V_s -anomaly beneath the Caribbean (Fig. 3F). Hutko et al. [31] recently reported seismic observations of a 100-km vertical step in the shear velocity discontinuity at the top of the D'' layer at the base of the mantle beneath the Cocos plate, which they interpreted as evidence of folded lithosphere. More quantitative estimates of the amplitude of such fold piles is probably not warranted at present, however. This is because slabs reaching the CMB will have lost much of their original thermal anomaly, and thus may be only slightly more viscous than the surrounding mantle. The buckling amplitude will therefore be strongly influenced by the external viscosity, an effect that is not included in the scaling laws shown in Fig. 2.

Buckling of subducted lithosphere in the transition zone has important implications for other aspects of mantle structure and dynamics. First, accounting for buckling enhances the likelihood of identifying correctly which ancient subducted plate corresponds to a given fast anomaly seen on a tomographic image [29,18]. By the same token, once particular slabs are clearly identified in tomographic images, their positions can be used to constrain the past positions of plate boundaries that have disappeared from Earth's surface. Buckling also has a significant effect on the time history of the distribution of density anomalies in Earth's mantle, which in turn controls the evolution of the planet's gravity field and angular momentum budget. Assuming that subduction of dense oceanic lithosphere creates most of Earth's internal density anomalies, Ricard et al. [32] calculated their distribution during the past ≈ 180 Ma from the known history of surface plate motions. Richards et al. [33] used a similar model to

estimate long-term variations of Earth's moment of inertia tensor, concluding that the low rate of true polar wander during the past 100 Ma reflects the slow rate of change in the large scale pattern of plate tectonic motions during Cenezoic and late Mesozoic time. Such calculations require assumptions about the trajectories followed by the sinking slabs and how much they thicken and slow down as they cross the transition zone. The correlation between paleo slab reconstructions and global tomography models suggests that the average velocity reduction factor of slabs entering the lower mantle is 2–7 [32]. Values at the higher end of this range agree well with our interpretations of the tomographic images beneath Central America and Java.

In conclusion, seismic tomography together with quantitative scaling laws from fluid dynamics suggests that subducted oceanic lithosphere can undergo a ‘periodic buckling’ instability when it encounters enhanced resistance during its descent into the mantle. At present, tomography is capable of resolving the wedge-shaped ‘envelope’ of the folded lithosphere, which has a characteristic lateral dimension >400 km. Clearly, the next step is to investigate the internal structure of the wedge, which is expected to comprise a layered pile of folds with a characteristic layer thickness ≈ 100 km. Resolving this finescale structure will require a new generation of regional tomographic models with higher resolution than is currently available.

Acknowledgements

This work was supported by the DyETI program of the Institut National des Sciences de l'Univers (INSU), France. We thank A. Davaille for helpful discussions, L. Guillou-Frotier for comments on the manuscript and for the photograph used in Fig. 1b, and an anonymous referee for a constructive review. This is IGP contribution number 2183.

References

- [1] G.I. Taylor, Instability of jets, threads, and sheets of viscous fluid, Proc. Twelfth Int. Cong. Appl. Mech. Springer Verlag, Berlin, 1968.
- [2] J.O. Cruickshank, Viscous fluid buckling: a theoretical and experimental analysis with extensions to general fluid stability, Ph. D. dissertation, Iowa State University, Ames, Iowa (1980).
- [3] R.W. Griffiths, J.S. Turner, Buckling of viscous plumes impinging on a density or viscosity interface, Geophys. J. 95 (1988) 397–419.
- [4] J.O. Cruickshank, Low-Reynolds-number instabilities in stagnating jet flows, J. Fluid Mech. 193 (1988) 111–127.
- [5] A.L. Yarin, B.M. Tchavdarov, Onset of buckling in plane liquid films, J. Fluid Mech. 307 (1996) 85–99.

- [6] M.F. Tome, S. McKee, Numerical simulation of viscous flow: buckling of planar jets, *Int. J. Numer. Methods Fluids* 29 (1999) 705–718.
- [7] M. Skorobogatiy, L. Mahadevan, Buckling of viscous sheets and filaments, *Europhys. Lett.* 52 (2000) 532–538.
- [8] N.M. Ribe, Periodic buckling of viscous sheets, *Phys. Rev., E Stat. Phys. Plasmas Fluids Relat. Interdiscip. Topics* 68 (2003) 036305.
- [9] J.B. Gaherty, B.H. Hager, Compositional vs. thermal buoyancy and the evolution of subducted lithosphere, *Geophys. Res. Lett.* 21 (1994) 141–144.
- [10] L. Guillou-Frottier, J. Buttles, P. Olson, Laboratory experiments on the structure of subducted lithosphere, *Earth Planet. Sci. Lett.* 133 (1995) 19–34.
- [11] U.R. Christensen, The influence of trench migration on slab penetration into the lower mantle, *Earth Planet. Sci. Lett.* 140 (1996) 27–39.
- [12] E. Tan, M. Gurnis, L. Han, Slabs in the lower mantle and their modulation of plume formation, *Geochem. Geophys. Geosyst.* 3 (2002) 1067, doi:10.1029/2001GC000238.
- [13] A.K. McNamara, P.E. van Keken, S.-I. Karato, Development of finite strain in the convecting lower mantle and its implications for seismic anisotropy, *J. Geophys. Res.* 108 (2003), doi:10.1029/2002JB001970.
- [14] A. Enns, T.W. Becker, H. Schmeling, The dynamics of subduction and trench migration for viscosity stratification, *Geophys. J. Int.* 160 (2005) 761–775.
- [15] N. Bellahsen, C. Faccenna, F. Funiciello, Dynamics of subduction and plate motion in laboratory experiments: insights into the “plate tectonics” behavior of the Earth, *J. Geophys. Res.* 110 (2005), doi:10.1029/2004JB002999.
- [16] H. Káráson, R. van der Hilst, Tomographic imaging of the lower mantle with differential times of refracted and diffracted core phases (PKP, Pdiff), *J. Geophys. Res.* 106 (2001) 6569–6587.
- [17] E.R. Engdahl, R. van der Hilst, R. Buland, Global teleseismic earthquake relocation with improved travel times and procedures for depth determination, *Bull. Seismol. Soc. Am.* 88 (1998) 722–743.
- [18] Y. Ren, E. Stutzmann, R. van der Hilst, J. Besse, Understanding seismic heterogeneities in the lower mantle beneath the Americas from seismic tomography and plate tectonic history, *J. Geophys. Res.* (in press).
- [19] B.L.N. Kennett, E.R. Engdahl, R. Buland, Constraints on seismic velocities in the Earth from travel times, *Geophys. J. Int.* 122 (1995) 108–124.
- [20] A. Replumaz, H. Káráson, R. van der Hilst, J. Besse, P. Tapponnier, 4-D evolution of SE Asia’s mantle from geological reconstructions and seismic tomography, *Earth. Planet. Sci. Lett.* 221 (2004) 103–115.
- [21] E. Stutzmann, J. Matas, Y. Ren, R. van der Hilst, Thermochemical structure of deep slabs beneath America derived from P and S wave tomography, *EOS Trans. Am. Geophys. Union* 86/(52) (2005) Fall Meet. Suppl., Abstract S33D-05.
- [22] A. Heuret, S. Lallemand, Plate motions, slab dynamics, and back-arc deformation, *Phys. Earth Planet. Int.* 149 (2005) 31–51.
- [23] Z. Garfunkel, C.A. Anderson, G. Schubert, Mantle circulation and the lateral migration of subducted slabs, *J. Geophys. Res.* 91 (1986) 7205–7223.
- [24] M. Gurnis, B.H. Hager, Controls of the structure of subducted slabs, *Nature* 335 (1988) 317–321.
- [25] R. Griffiths, R.I. Hackney, R.D. van der Hilst, A laboratory investigation of effects of trench migration on the descent of subducted slabs, *Earth Planet. Sci. Lett.* 133 (1995) 1–17.
- [26] K.M. Fischer, T.H. Jordan, K.C. Creager, Seismic constraints on the morphology of deep slabs, *J. Geophys. Res.* 93 (1988) 4773–4783.
- [27] K.M. Fischer, K.C. Creager, T.H. Jordan, Mapping the Tonga slab, *J. Geophys. Res.* 96 (1991) 14,403–14,427.
- [28] J.E. Vidale, D. Garcia-Gonzalez, Seismic observation of a high-velocity slab 1200–1600 in depth, *Geophys. Res. Lett.* 15 (1988) 369–372.
- [29] S. Grand, Mantle shear structure beneath the Americas and surrounding oceans, *J. Geophys. Res.* 99 (1994) 11591–11621.
- [30] Y. Fukao, S. Widiyantoro, M. Obayashi, Stagnant slabs in the upper and lower mantle transition region, *Rev. Geophys.* 39 (2001) 291–323.
- [31] A.R. Hutko, T. Lay, E.J. Garnero, J. Revenaugh, Seismic detection of folded, subducted lithosphere at the core–mantle boundary, *Nature* 441 (2006) 333–336.
- [32] Y. Ricard, M. Richards, C. Lithgow-Bertelloni, Y. le Stunff, A geodynamic model of mantle density heterogeneity, *J. Geophys. Res.* 98 (1993) 21,895–21,909.
- [33] M. Richards, Y. Ricard, C. Lithgow-Bertelloni, G. Spada, R. Sabadini, An explanation for Earth’s long term rotational stability, *Science* 275 (1997) 372–375.